Supplementary Material
Biaxial, Twist-bend and Splay-bend Nematic Phases of Banana-shaped Particles revealed by lifting the "Smectic Blanket"

Massimiliano Chiappini, Tara Drwenski, René van Roij, and Marjolein Dijkstra

I. MODEL AND SIMULATION METHODS FOR BENT AND CURVED RODS

We perform Monte Carlo simulations on systems of hard bent spherocylinders and of hard curved spherocylinders. The bent spherocylinders consist of two hard spherocylinders and a capping sphere (see Fig. 1 (c) of the Letter). In order to check for overlaps between bent rods, we employ the overlap test for the individual spherocylinders of which they are composed. The overlap test for spherocylinders is extensively discussed in Ref. [1]. For computational convenience, we model the curved rods of length-to-diameter ratio L/D and opening angle Ψ by $N_s = 2L/D$ spherical beads of diameter D equally spaced along an arc of circle of radius $R = L/2\cos(\Psi/2)$ and length $l = 2(\pi - \Psi)R$, see Fig. 1 of the SM. The overlap between two curved rods is tested by checking the overlap of any pair of spherical beads composing the curved rods. This overlap algorithm scales with the number of spheres in the system when a cell list is employed. To speed up equilibration, we implement the cell list method for both model systems [2]. The cell list method is straighforwardly applied to the spheres of which the curved rods are composed. In the case of the bent spherocylinders, we mesh the particle by spheres and check overlaps between the meshing spheres using the cell list as a pre-test for the overlap between bent spherocylinders. As the bead model exhibits an artificial corrugation compared to the smooth curved rod, we checked our results on the phase behavior by doubling the number of spheres. We observe no change in phase behavior by increasing the number of beads, but we find that the equations of state are slightly shifted to smaller packing fractions as the particle volume increases with the number of beads.

In order to determine the equations of state and the phase behavior, we perform both compression and expansion runs using standard NPT Monte Carlo simulations with periodic boundary conditions, starting from a random isotropic low-density state and from the close-packed crystal state, respectively. To predict the close-packed crystal state, we employ the floppy box Monte Carlo method [3, 4]. Since the unit cell of these crystal structures are in general non-orthorhombic, we use the variable box shape Monte Carlo method. The number of particles in the simulation box strongly depends on the particle model, the starting close-packed crystal structure and the expected phases, in order to achieve the best trade-off between accuracy and computational efficiency. In general, system sizes from $N = 1024$ to $N = 4096$ are employed. Along the equilibration in both compression and expansion runs a wide set of observables is measured (the packing fraction, the uniaxial order parameters, the smectic order parameters, etc.). The equilibration is considered complete when the order parameters cease to drift and only fluctuate around a mean value. The duration of the equilibration strongly depends on the particle shape and the equilibrated phase, but is typically of the order of 10^6 to 10^8 MC cycles.

To map out the phase diagram of crooked rods of aspect ratio $L/D = 5$ as a function of the opening angle Ψ we measure the equations of state of the system at every 5° ($\Psi = 0°$, 5°, 10°, etc.). To construct the phase diagram of crooked rods of aspect ratio $L/D = 10$ we determine the equation of state for the set of opening angles $\Psi = 0°$, 2.5°, 5°, 7.5°, 10°, 12.5°, 15°, 20°, 25°, 30°, 45°, 60°, 75°, 90°, 105°, 130°, 135°, 140°, 150°, 155°, 160°, 170°, and 180°.

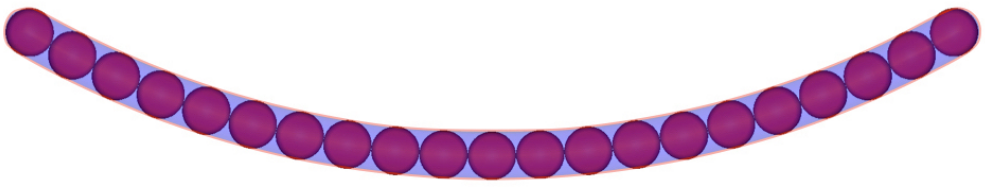

FIG. 1: Hard curved spherocylinder with a length-to-diameter ratio of $L/D = 10$ and $\Psi = 150°$ as modeled by hard spherical beads.

II. PHASE DIAGRAM OF HARD BENT SPHEROCYLINDERS OF ASPECT RATIO L/D = 5

In Fig. 2 of the SM we report the phase diagram of hard bent spherocylinders of aspect ratio $L/D = 5$ as a function of the opening angle Ψ and the packing fraction η, as discussed in the Letter.

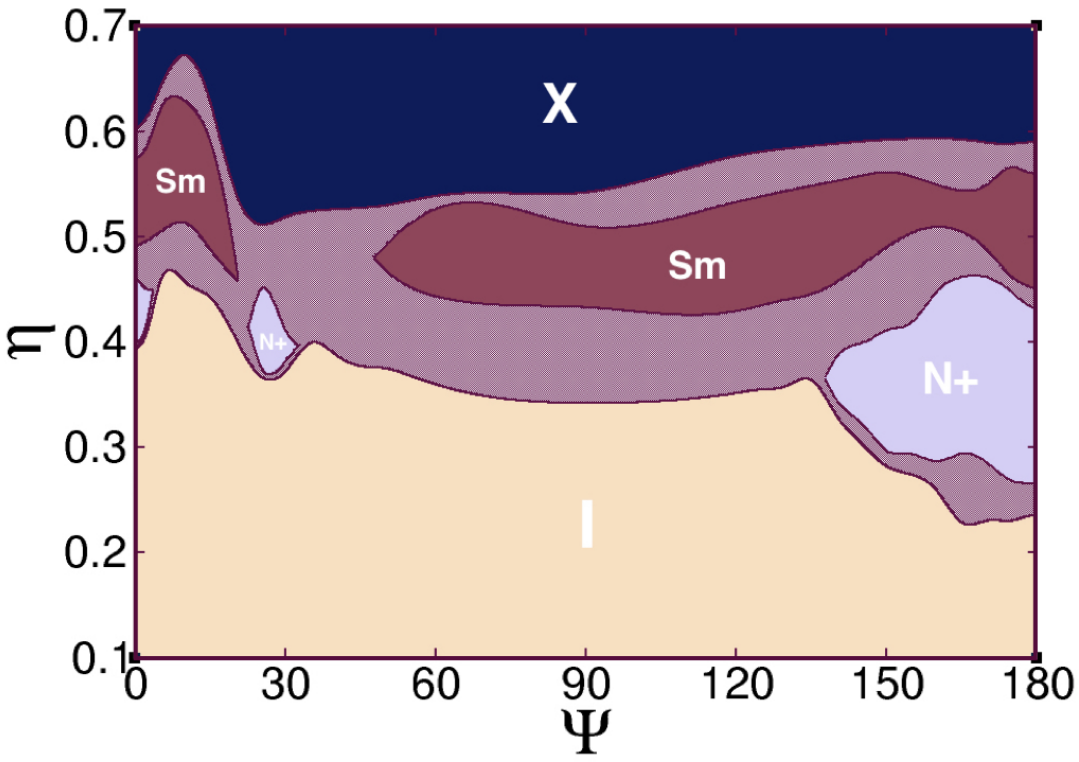

FIG. 2: Phase diagram of hard bent spherocylinder with a length-to-diameter ratio of $L/D = 5$.

III. PHASE DIAGRAM OF A POLYDISPERSE SYSTEM OF HARD BENT SPHEROCYLINDERS

We also determine the phase diagram for a system of hard bent spherocylinders with a Gaussian length distribution, a mean length $\langle L \rangle = 10D$ and a standard deviation $\sigma_L = 0.36\langle L \rangle$ using Monte Carlo simulations. The length of the particles in the system is drawn initially from a Gaussian distribution and then kept fixed along the simulation. We do not allow for demixing and fractionation. In order to distinguish between rod-like prolate nematic N_+, plate-like oblate nematic N_-, and biaxial nematic N_b phases, we measure the orientational order of the three orthogonal particle axes as depicted in Fig. 3 in the SM, i.e. the axis **n** (the prolate axis for $\Psi > 90°$), the polar axis **m** (the prolate axis for $\Psi < 90°$), and the oblate axis **o** (aligned in the platelet-like oblate nematic phase N_- and/or in the biaxial nematic N_b phase, where all the axes are simultaneously aligned). Note that particle axes are considered to be aligned if the corresponding uniaxial order parameter is larger than 0.6. Simulations are performed for the discrete set of opening angles $\Psi = 0°$, $30°$, $45°$, $60°$, $75°$, $90°$, $105°$, $120°$, $145°$, $150°$, and $180°$, resulting in the phase diagram in Fig. 2b of the Letter. Here, we show in Fig. 4 of the SM the actually simulated data.

We observe that the I-N phase transition is always driven by orientational order of the prolate particle axes (either **n** or **m**, respectively, for $\Psi > 90°$ and $\Psi < 90°$). The other particle axes become more aligned upon further increasing the packing fraction η, stabilizing the N_b phase at sufficiently high η. The orientational order of the secondary particle axes becomes more pronounced when the particles become more bent, showing no orientational order of the secondary particle axes at $\Psi \simeq 0°$ or $\Psi \simeq 180°$, when the particle shape is actually uniaxial and the secondary axis is not even defined, and strong alignment of both particle axes at intermediate opening angles, resulting into a direct transition from the I to the N_b phase. Consequently, we find a single cusp-shaped N_b phase ending in a Landau critical point at $\Psi = 105°$ sandwiched between two N_+ phases for $\Psi > 105°$ and $\Psi < 105°$. We show a typical N_b state in Fig. 5

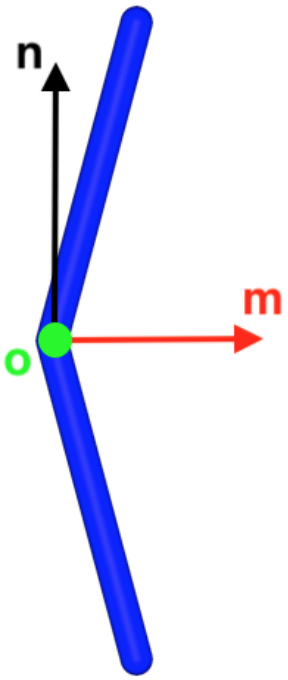

FIG. 3: The three particle axes **n**, **m**, and **o** of a bent spherocylinder.

of the SM.

IV. RECOGNIZING THE TWIST- AND SPLAY-BEND NEMATIC PHASES

To the best of our knowledge, simple and unique order parameters for the deformed N_{TB} and N_{SB} do not exist in literature. Although the transitions to the N_{TB} and N_{SB} phases are signalled by typical features of the ordinary order parameters (the $N - N_{TB}$ phase transition is associated to an instantaneous drop of the prolate uniaxial order parameter while the $N_{TB} - N_{SB}$ phase transition is associated by an abrupt increase of the prolate uniaxial order parameter, as shown later), to unequivocally recognise these phases we check for their main fingerprint: the modulation of the nematic director field. In Fig. 6a and 6b of the SM we show examples of the modulation of the nematic director field $\hat{\mathbf{n}}(z) = (n_x(z), n_y(z), n_z(z))$ along the phase axis respectively for a N_{TB} and a N_{SB} phase, along with a fit of the theoretical modulation. From the fit we can measure the pitch length p and the cone angle θ_0 of the phase.

In particular, the modulation of the nematic director field of the N_{SB} phase is constrained to a plane. In the Letter, the modulation is defined in the yz-plane, namely as $\hat{\mathbf{n}}(z) = \sin(\theta_0 \sin(qz))\ \mathbf{e}_y + \cos(\theta_0 \sin(qz))\ \mathbf{e}_z$, but this choice is arbitrary. In general, a N_{SB} with the director along the z-axis can be modulated within any plane that contains the z-axis, at an angle Φ with the x-axis (for example, $\Phi = 45°$ in Fig. 6b of the SM). Therefore, the modulation that we actually have to fit on the simulation data is $\hat{\mathbf{n}}(z) = -\sin\Phi \sin(\theta_0 \sin(qz))\ \mathbf{e}_x + \cos\Phi \sin(\theta_0 \sin(qz))\ \mathbf{e}_y + \cos(\theta_0 \sin(qz))\ \mathbf{e}_z$.

V. PITCH AND CONE ANGLE OF THE TWIST- AND SPLAY-BEND NEMATIC PHASES

In Fig. 7 (a-d) of the SM we show the pitch and cone angle as a function of the packing fraction of the N_{TB} phase of monodisperse crooked rods of aspect ratio $L/D = 10$ and opening angles $\Psi = 130°$, $135°$, $140°$, and $150°$, respectively. In Fig. 8a and Fig. 8b of the SM we show the packing fraction dependence of the pitch and cone angle of, respectively, the N_{TB} and N_{SB} phases of curved spherocylinders with $L/D = 10$ and $\Psi = 150°$.

In the N_{TB} phase — both for bent and curved spherocylinders — the pitch length decreases and the cone angle increases upon moving deeper into the N_{TB} phase (increasing packing fraction), consistent with previous literature results. In particular, the data for $\Psi = 130°$, $135°$, and $140°$ are in good qualitative and quantitative agreement with the theoretically predicted pitch length values for bent mesogens with the same opening angles (Ref. [23] of the Letter), whereas the cone angle values are typically smaller than obtained from theory.

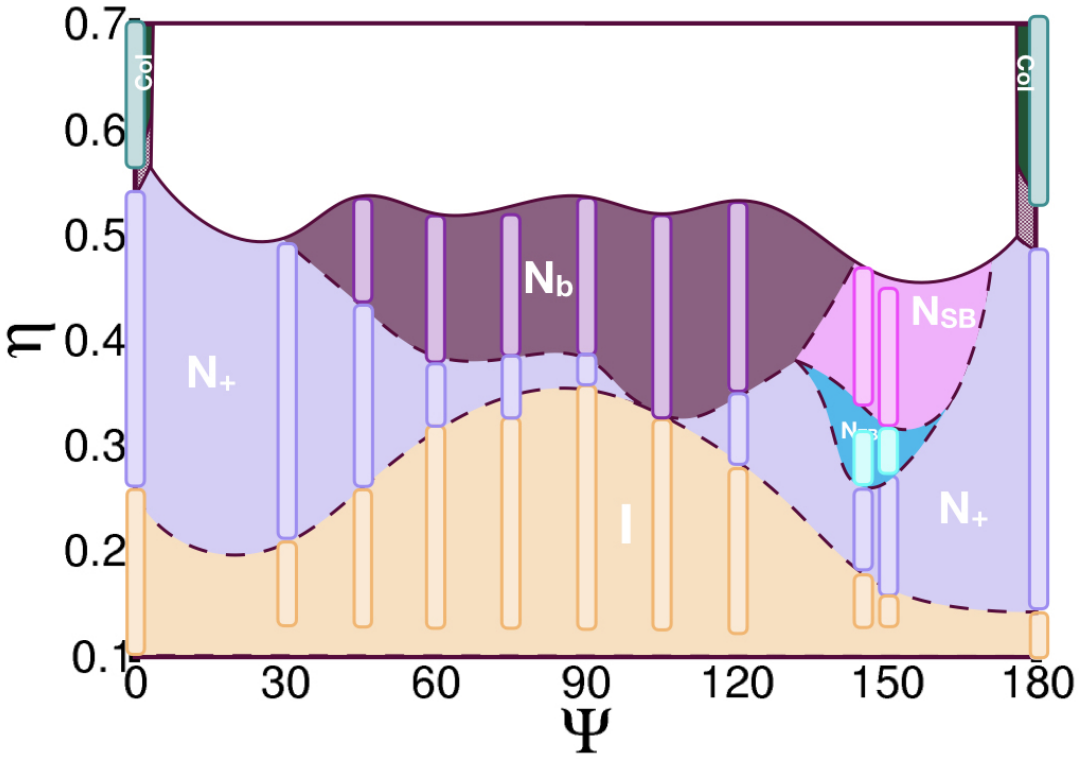

FIG. 4: Phase diagram of polydisperse hard bent spherocylinders with a Gaussian length distribution, an average length $\langle L\rangle = 10D$ and polydispersity $\sigma_L = 0.36\langle L\rangle$ in the packing fraction η - opening angle Ψ representation as reported in Fig. 2b of the Letter, displaying I (yellow), N_+ (lilac), Sm (red brown), columnar Col (dark green), and crystal X (dark blue) phases, but also twist-bend N_{TB} (light blue), biaxial N_b (purple), and splay-bend N_{SB} (pink) nematic phases. The white region corresponds to unexplored parts of the phase diagram. Dashed lines correspond to continuous transitions. The bars correspond to the actually simulated data points.

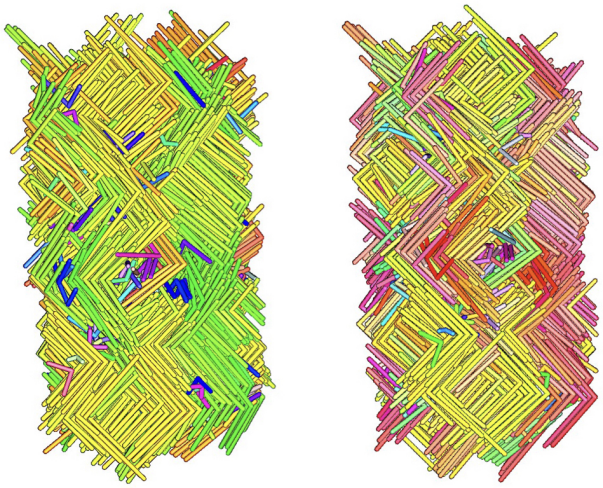

FIG. 5: Snapshot of a biaxial nematic N_b phase of polydisperse hard bent spherocylinders with opening angle 90°, $\langle L\rangle = 10D$ and $\sigma_L = 0.36\langle L\rangle$ at $\eta = 0.45$, on the left colored according to the orientation of the prolate axis $\hat{\mathbf{n}}$, on the right colored according to the orientation of the oblate axis $\hat{\mathbf{o}}$.

On the other hand, in the N_{SB} phase both the pitch and cone angle decrease with packing fraction.

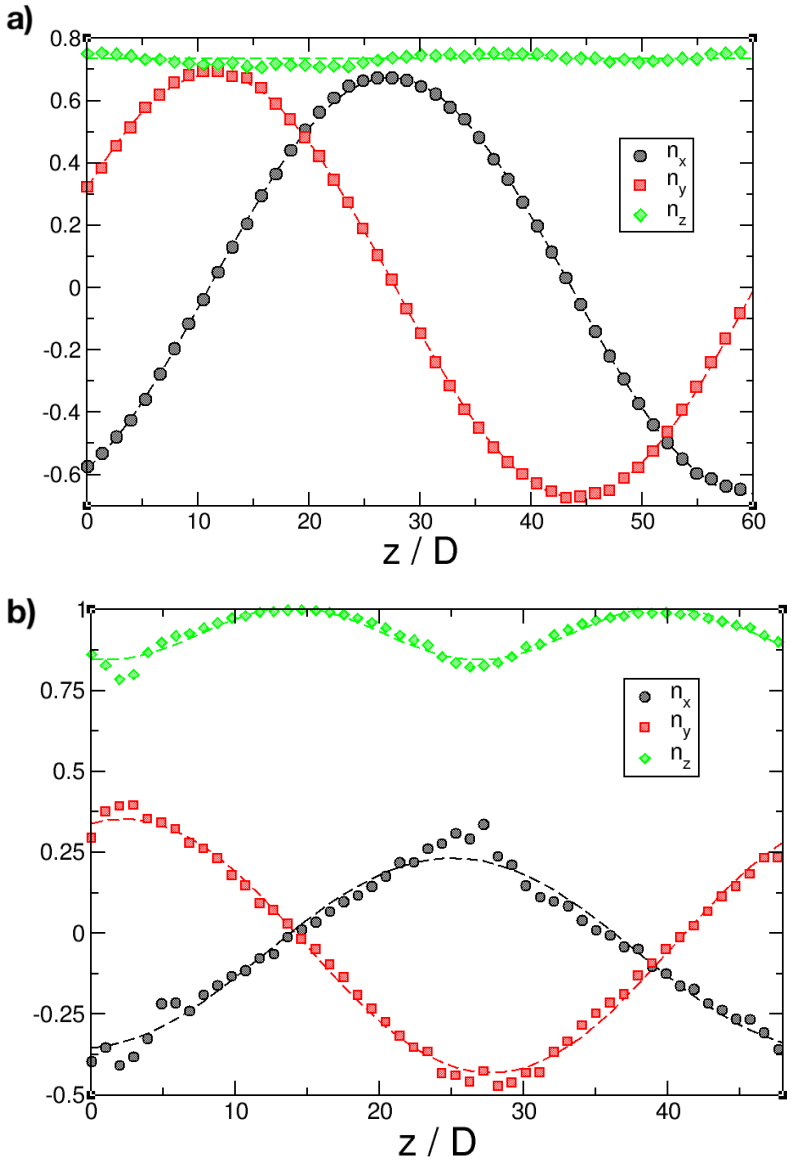

FIG. 6: Modulation of the x, y, and z components (black, red and green symbols, respectively) of the nematic director field $\hat{\mathbf{n}}(z) = (n_x(z), n_y(z), n_z(z))$ in a (a) N_{TB} phase and (b) N_{SB} phase of curved spherocylinders at packing fraction $\eta = 0.370$ and $\eta = 0.38$, respectively. The dashed lines are fits of the theoretical expression for the nematic director field.

VI. EQUATIONS OF STATE FOR HARD BENT SPHEROCYLINDERS AND HARD CURVED SPHEROCYLINDERS

We present the phase diagram of hard bent spherocylinders and hard curved spherocylinders of aspect ratio $L/D = 10$ and opening angle $\Psi = 150°$ in Fig. 5 of the Letter. We plot the corresponding equations of state, i.e., the pressure $\beta P v_0$ as a function of packing fraction η (in black) in Fig. 9(a,b) of the SM along with the nematic order parameter S (in red) and the smectic order parameter τ (in green) as defined in Ref. [5], where v_0 denotes the particle volume and $\beta = 1/k_B T$ the inverse temperature. We observe a clear jump in the nematic order parameter S at the isotropic I - nematic N transition as well as a drop in S at the N to twist-bend nematic N_{TB} phase transition for both the bent and curved spherocylinders. At higher packing fractions, we find a clear discontinuity of the smectic order parameter at the first-order $N_{TB} - Sm$ phase transition for hard bent spherocylinders. In the case of hard curved spherocylinders, the smectic order parameter gradually increases with η as the phase transition from a splay-bend nematic N_{SB} phase without any layering to a smectic Sm phase in which the particles are arranged in smectic layers is continuous.

In particular, in Fig. 10 (a) of the SM we show the evolution of the density profile for various packing fractions η,

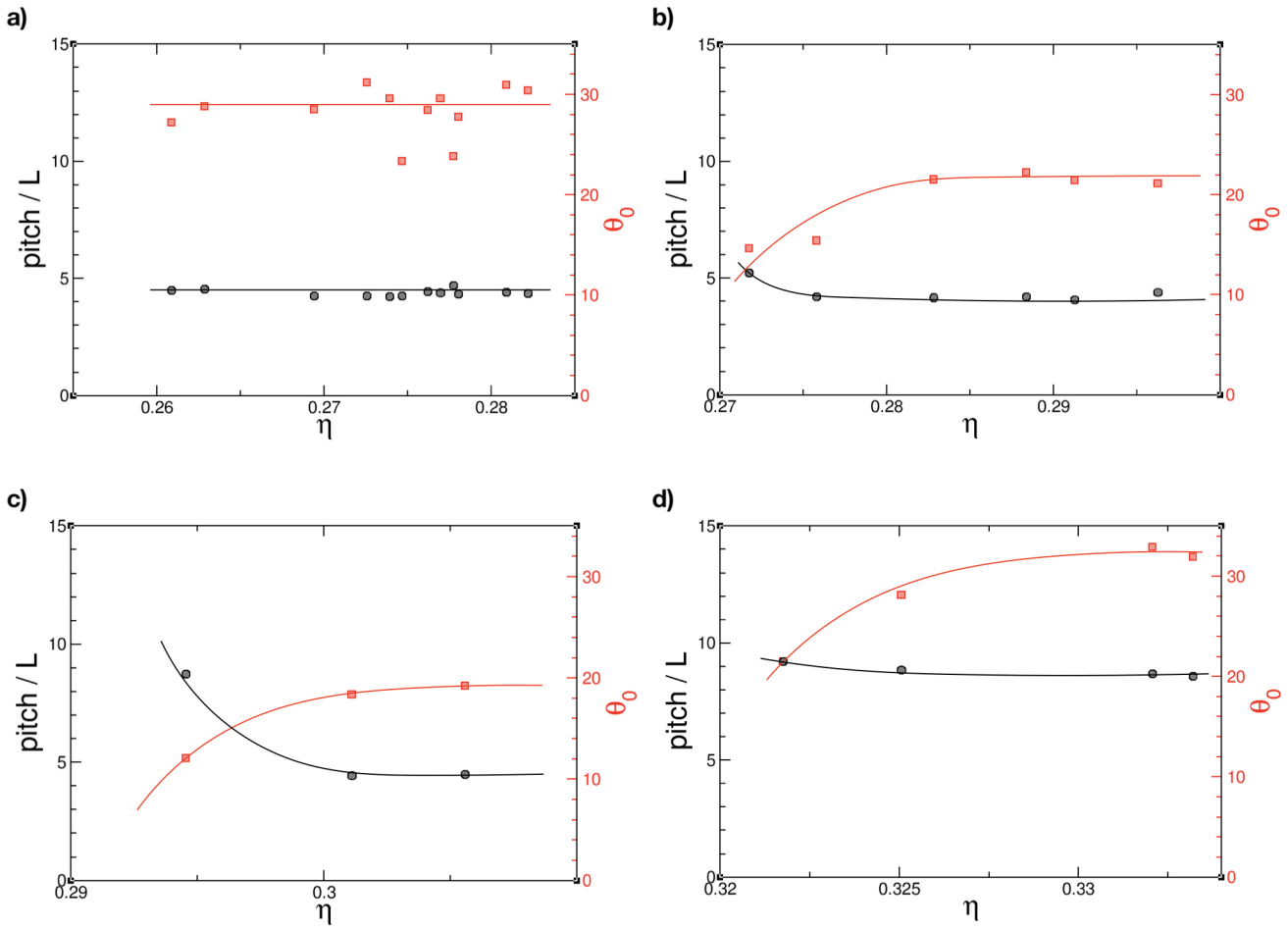

FIG. 7: The pitch length p (black) and the cone angle θ_0 (red) as a function of packing fraction η of the N_{TB} phase of bent spherocylinders with aspect ratio $L/D = 10$ and opening angle $\Psi = 130°$ (a), $135°$ (b), $140°$ (c), and $150°$ (d). The lines are guides to the eye.

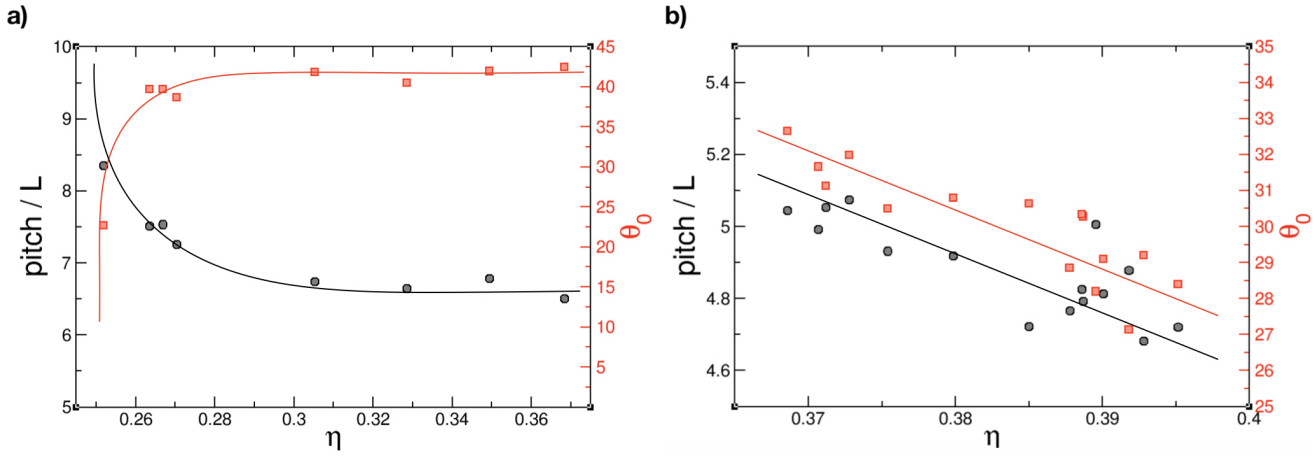

FIG. 8: The pitch length p (black) and the cone angle θ_0 (red) as a function of packing fraction η of (a) the N_{TB} and (b) the N_{SB} phase of curved spherocylinders with aspect ratio $L/D = 10$ and opening angle $\Psi = 150°$. The lines are guides to the eye.

showing the effect of a continuous transition from the N_{SB} to the Sm phase. The development of the peaks in the density distribution corresponds to an increase of the smectic order parameter. The density profiles in Fig. SM 10(a) feature a periodic modulation, but should be spatially uniform in the nematic N_{SB} phase. This leads to values of the smectic order parameter τ which are relatively high for a nematic phase (see Fig. 9 (b) of the SM). The spatial density modulations are possibly caused by the presence of the(near-)critical $N_{SB} - Sm$ transition, which gives rise to critical fluctuations that exceed the size of the simulation box. Increasing the size of the simulation box in the direction of the nematic director should suppress the spatial modulations. In Fig. SM 10(b) we show that in a longer simulation box the density profile $\rho(z)$ along the nematic director of a N_{SB} phase at a packing fraction $\eta = 0.38$ shows no spatial modulations, whereas the nematic director field $\mathbf{n}(z)$ is clearly spatially modulated, thereby confirming that the density modulations in the N_{SB} phase in Fig. SM 10(a) are caused by finite-size effects. An accurate study of the finite-size scaling of the $N_{SB} - Sm$ phase transition of hard curved rods is beyond the scope of the present work.

Since the phase behaviour of hard bent spherocylinders with an aspect ratio $L/D = 10$ presented in Fig. 2a of the Letter can be divided into four distinct regions of opening angles with distinct phase sequences, $I - N_+ - Sm - X$ for $\Psi \lesssim 12.5°$, $I - N_+ - X$ for $12.5° \lesssim \Psi \lesssim 45°$, $I - Sm - X$ for $45° \lesssim \Psi \lesssim 120°$, and $I - N_+/N_{TB} - Sm - X$ for $\Psi \gtrsim 120°$, we show in Fig. 11 of the SM exemplary equations of state for each of these regions, i.e. for opening angles $\Psi = 5°$, $20°$, and $105°$. The one for $\Psi = 150°$ has already been shown in Fig. 9a of the SM.

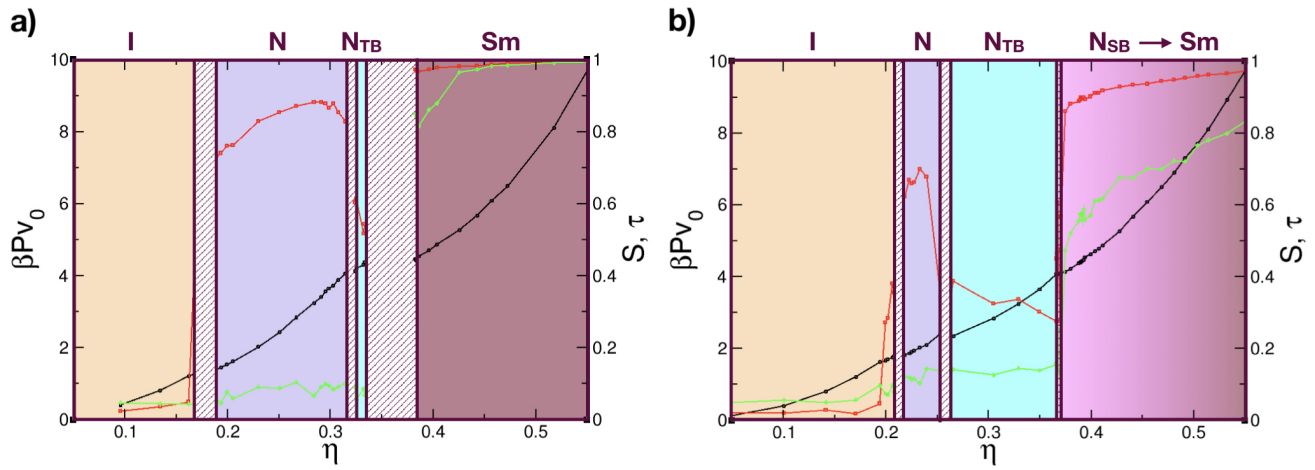

FIG. 9: Equation of state (black), i.e. pressure $\beta P v_0$ versus packing fraction η, with the scale on the left, of hard (a) bent and (b) curved spherocylinders with $L/D = 10$ and $\Psi = 150°$ along with the nematic order parameter S (in red) and the smectic order parameter τ (in green) with the scale on the right.

VII. THE CONTINUOUS $I - N - N_b$ TRANSITION OF POLYDISPERSE BENT SPHEROCYLINDERS

The phase diagram in Fig. 2b of the Letter presents dashed lines corresponding to continuous $I - N - N_b$ phase transitions of systems of polydisperse hard bent spherocylinders, in which the uniaxial order parameters associated to the different particle axes gradually increase upon compression (see Sect. SM III) without any significant discontinuity in the equation of state. A closer inspection of the states along the compression route shows that the continuous transition is driven by the formation, growth and aggregation of clusters of highly ordered particles, as shown in Fig. SM 12. In particular, the presence of Sm clusters of particles with short-range positional order across the whole nematic range in systems of bent particles, supposedly caused by their frustrated translational symmetry, is well known in literature and widely confirmed in experiments [6]. In systems of monodisperse particles, these clusters aggregate into structures with long-range positional order, yielding stable Sm phase. In systems of polydisperse particles, the coherent aggregation of these clusters is hindered by their different length scales, and the stable Sm phase is frustrated into a N_b phase composed of clusters of particles with short-range positional order.

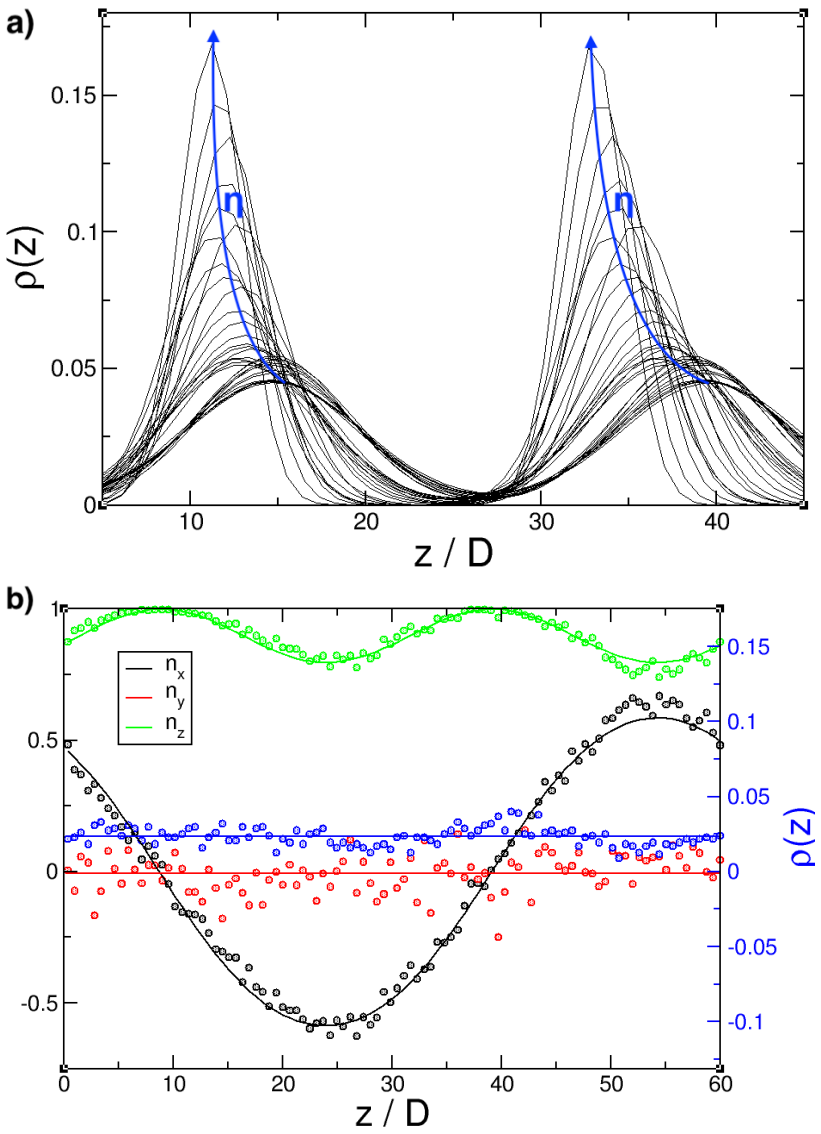

FIG. 10: (a) Density profile $\rho(z)$ for various packing fractions ($\eta = 0.38 \rightarrow 0.6$) along the continuous $N_{SB} \rightarrow Sm$ phase transition of hard curved spherocylidners with $L/D = 10$ and $\Psi = 150°$. (b) The $x-$, $y-$, and $z-$ components of the nematic director field $\mathbf{n}(z)$ (black, red, and green, left axis) and the density profile $\rho(z)$ (blue, right axis) of a N_{SB} phase at packing fraction $\eta = 0.38$ in a longer simulation box, which presents no modulation of the density profile.

VIII. MONTE CARLO SIMULATIONS IN THE SEMI-GRAND CANONICAL ENSEMBLE

In the Letter, we discuss a MC scheme that is based on the Semi-Grand Canonical Ensemble (SGCE) and the Non-Equilibrium Potential Refinement (NEPR) method. This method involves two SGCE simulations with a fixed number of particles, the same pressure and temperature, and the same tunable distribution of chemical potentials $\mu(L)$ of particle species. The distribution $\mu(L)$ is tuned iteratively via the NEPR algorithm such that the overall distribution of the particle lengths in both simulation boxes together is a Gaussian parent distribution with an imposed average $\langle L \rangle$ and standard deviation σ_L, in principle allowing for the system to demix and fractionate into two coexisting phases of different density and different length distributions if favourable.

We consider a system of hard bent spherocylinders of aspect ratio $L/D = 10$ and opening angle $\Psi = 90°$, which displays an $I - Sm - X$ phase sequence for the monodisperse system as can be seen from the phase diagram in Fig. 2a of the Letter. We simulate such a system in two simulation boxes at various pressures across the $I - Sm$ phase transition with increasing polydispersity. We find that the two simulation boxes show two I phases, a coexistence of I and Sm phases, and two Sm phases upon increasing pressure at low polydispersity, i.e. $\sigma_L = 0.01\langle L \rangle$. At high

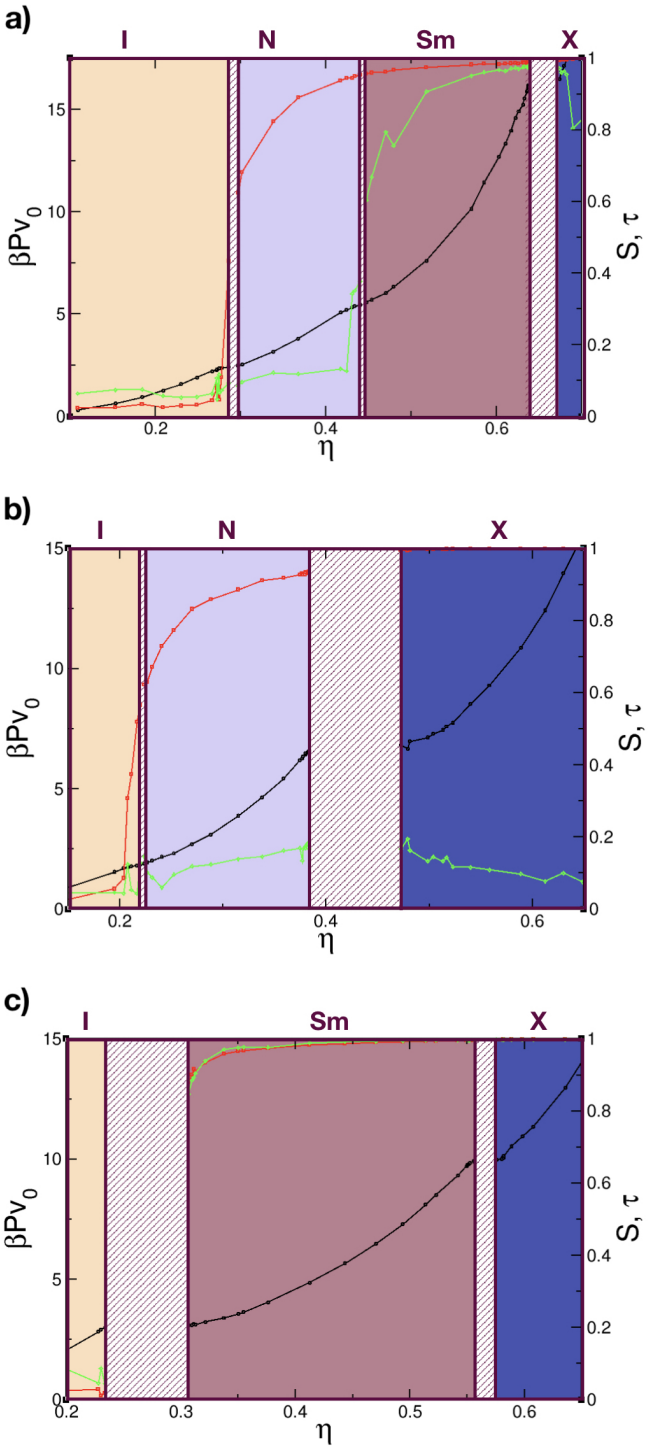

FIG. 11: Equations of state (black), i.e. pressure $\beta P v_0$ versus packing fraction η, with the scale on the left, of hard bent spherocylinders with $L/D = 10$ and $\Psi = 5^\circ$ (a), 20° (b), and 105° (c) along with the nematic order parameter S (in red) and the smectic order parameter τ (in green) with the scale on the right.

polydispersity, i.e. $\sigma_L = 0.36\langle L\rangle$, we find in both simulation boxes states along the continuous $I - N - N_b$ transition with increasing pressure, without any fractionation.

On the other hand, starting with a monodisperse system at a pressure corresponding to the $I - Sm$ coexistence and gradually increasing the polydispersity we find that the $I - Sm$ phase coexistence remains at intermediate

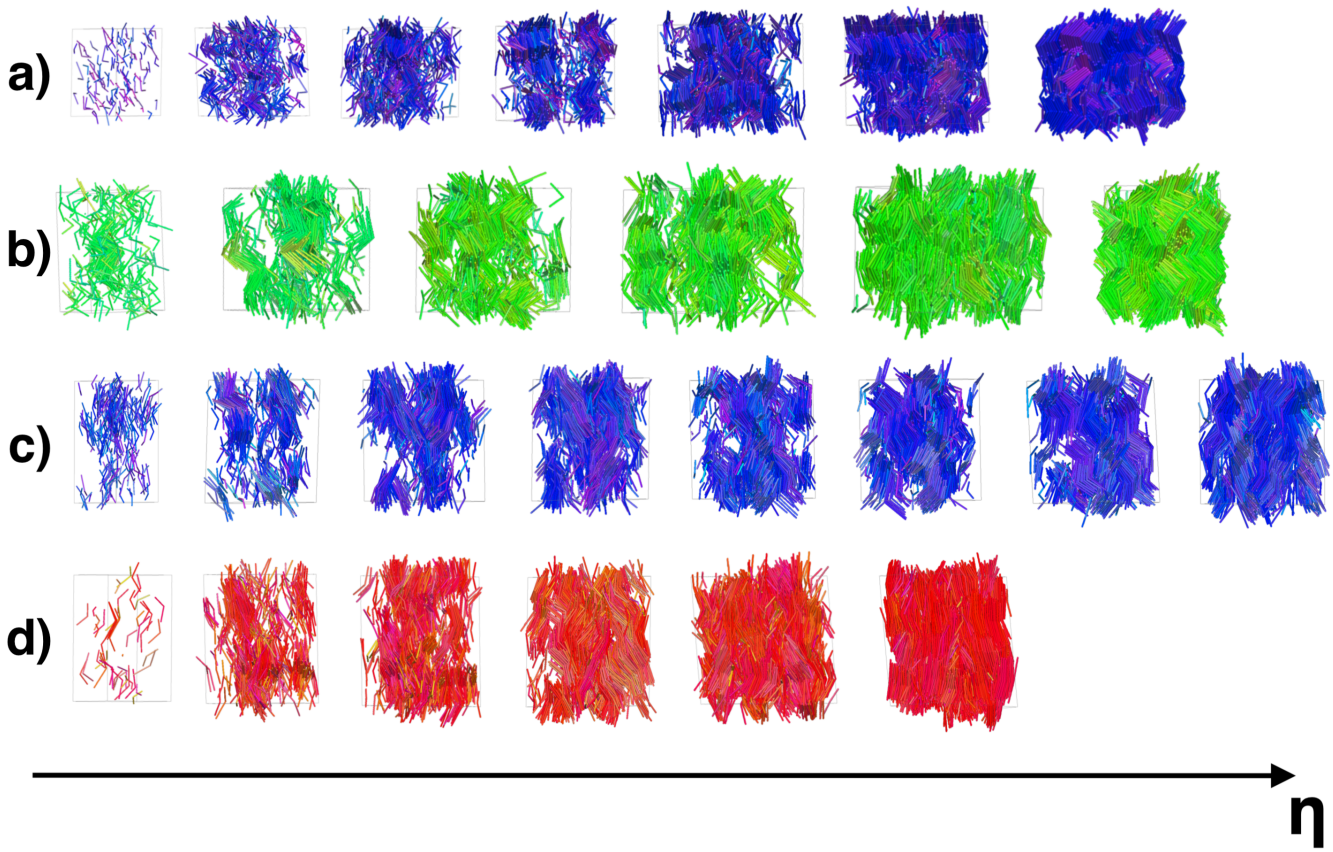

FIG. 12: Snapshots along the continuous $I-N-N_b$ transition of polydisperse hard bent spherocylinders with a distribution of particle lengths of mean $\langle L\rangle/D = 10$ and standard deviation $\sigma_L = 0.36\langle L\rangle$, and opening angles (a) $\Psi = 60°$, (b) $75°$, (c) $90°$, and (d) $105°$. Only the particles with all axes (see Sect. SM III) significantly aligned are represented, showing the continuous formation, growth and aggregation of smectic clusters in the I phase which drives the continuous transition towards the N_b phase. The particles are coloured according to the orientation of the **n** axis.

polydispersities, but with a small degree of fractionation, and melts into two states along the continuous $I-N-N_b$ transition without fractionation at higher polydispersities, as shown in Fig. SM 13.

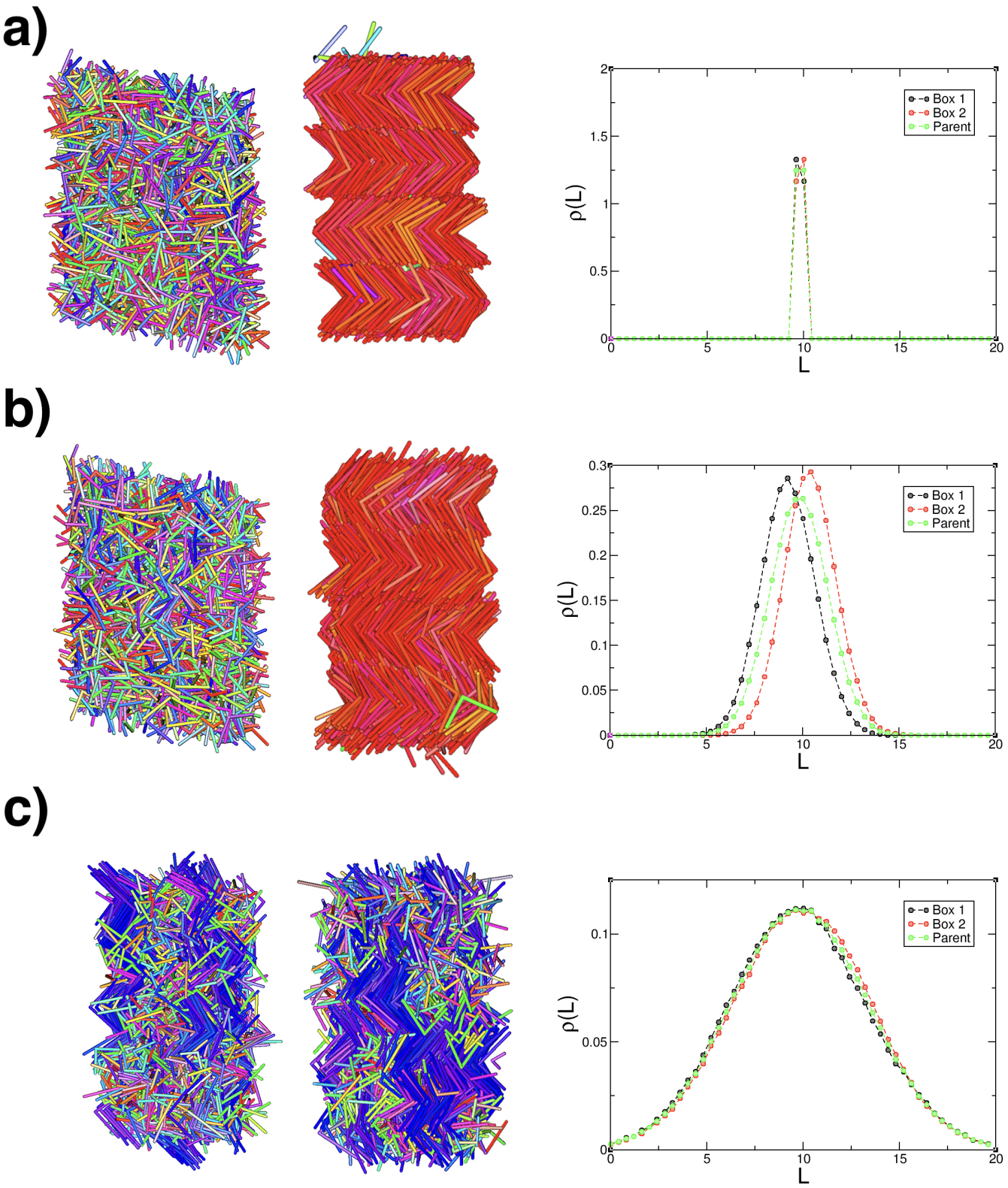

FIG. 13: Simulations in the SGCE (with the NEPR method) of coexisting $I - Sm$ states of polydisperse hard bent spherocylinders of aspect ratio $\langle L\rangle/D = 10$ and opening angle $\Psi = 90°$ for increasing polydispersities, from (a) $\sigma_L = 0.01\langle L\rangle$, to (b) $\sigma_L = 0.15\langle L\rangle$, to (c) $\sigma_L = 0.36\langle L\rangle$. On the left, we report snapshots of the simultaneously simulated boxes (left: box 1; right: box 2). On the right, we report the distributions of particle lengths in the boxes 1 and 2 (in black and red respectively) and the parent distribution of lengths (in green). The $I - Sm$ coexistence, stable without fractionation at low polydispersity (a), remains stable at intermediate polydispersities, but some degree of fractionation appears (b). At large polydispersities (c), the coexisting I and Sm states melt into two I states without fractionation. The coexisting I states show the presence of Sm clusters signature of the continuous $I - N$ transition of polydisperse bent spherocylinders (see Sect. VII).

[1] M. P. Allen, G. T. Evans, D. Frenkel, and B. M. Mulder, *Hard Convex Body Fluids* (John Wiley & Sons, Ltd, 2007), pp. 1–166, ISBN 9780470141458.
[2] D. Frenkel and B. Smit, *Understanding molecular simulation: from algorithms to applications* (Elsevier, 2001).
[3] L. Filion, M. Marechal, B. van Oorschot, D. Pelt, F. Smallenburg, and M. Dijkstra, PRL **103**, 188302 (2009).
[4] J. de Graaf, L. Filion, M. Marechal, R. van Roij, and M. Dijkstra, J. Chem. Phys. **137**, 214101 (2012).
[5] H. E. Bakker, S. Dussi, B. L. Droste, T. H. Besseling, C. L. Kennedy, E. I. Wiegant, B. Liu, A. Imhof, M. Dijkstra, and A. van Blaaderen, Soft Matter **12**, 9238 (2016).
[6] A. Jákli, O. D. Lavrentovich, and J. V. Selinger, Rev. Mod. Phys. **90**, 045004 (2018).